


 Cite this: *Nanoscale*, 2025, **17**, 23940

 Received 29th July 2025,
Accepted 26th September 2025

DOI: 10.1039/d5nr03212a

rsc.li/nanoscale

Reactive deposition of Pt single-atoms on g-C₃N₄: effect of Pt-precursors

 Nawres Lazaar,^{a,b} Shanshan Qin,^a Abdessalem Hamrouni,^{b,e} Hinda Lachheb,^b Jan Kolařík,^c Xuemei Zhou^{id}*^d and Patrik Schmuki^{id}*^{a,c}

Anchoring Pt single atoms (SAs) as co-catalysts on g-C₃N₄ has emerged as a promising approach to enhance the hydrogen production performance of this photocatalytic system. Particularly, by so-called reactive deposition, a maximum hydrogen evolution reaction performance can be achieved using a minimum amount of Pt loading. In this study, we explore the effects of different platinum (Pt) precursors on the reactive deposition of SAs onto g-C₃N₄, aiming to optimize the performance in photocatalytic hydrogen production. By examining a variety of Pt precursor types, we highlight critical parameters influencing deposition, including precursor charge, solution pH, ionic strength, and ligand properties. Our results reveal that precursors bearing anionic charges are distinctly more effective than cationic precursors for depositing highly active Pt SAs. Crucially, we find that the surface deposition reaction strongly depends on the ligand involved, with chloride-based complexes enabling more efficient Pt attachment compared to bromide-based complexes. Notably, variations in the oxidation state of platinum (Pt⁴⁺ versus Pt²⁺) did not significantly influence deposition outcomes. Among all precursors studied, (NH₄)₂[PtCl₆] achieved the highest catalytic activity, with optimal Pt loading (~0.026 wt%) and superior hydrogen evolution rates surpassing the widely utilized H₂[PtCl₆] precursor. Furthermore, adjustments to solution conditions, such as significant pH changes due to increased ionic strength, were found to negatively impact deposition and catalytic effectiveness. These insights underscore the

importance of precursor selection and solution chemistry control, providing a robust basis for the development of efficient and cost-effective single-atom photocatalysts formed by adsorption–reaction treatments.

1. Introduction

Photocatalytic H₂ generation from aqueous media, employing semiconductor materials has garnered considerable research interest as a promising strategy for sustainable green fuel generation.^{1–5} In recent years, graphitic carbon nitride (g-C₃N₄) has emerged as a highly attractive semiconductor, offering a suitable band structure for visible light water splitting as well as an excellent stability, and high structural flexibility for modification.^{6–9} However, for single-phase g-C₃N₄, the actual hydrogen production efficiency often falls short of expectations, primarily due to the fast recombination of charge carriers and slow reaction kinetics at the semiconductor-solution interface, even if hole transfer is aided by the use of sacrificial agents.^{10–13}

To overcome these limitations, the integration of suitable charge-transfer co-catalysts has been extensively explored. Platinum (Pt), in particular, has been widely identified as excellent co-catalyst for photocatalytic H₂ generation, when decorated or incorporated as nanoparticles, nanoclusters, or single atoms (SAs) on g-C₃N₄ surfaces.^{14–18}

In order to minimize cost, minimizing the catalysts size, and thus particularly Pt in the form of SAs, has recently attracted wide attention. Various synthesis approaches for Pt SAs have been reported, including wet immersion techniques, as well as gas-phase physical and chemical approaches.^{19–23} However, not all approaches deliver highly active SAs, *i.e.* depending on the synthesis approach, considerable amount of less active and hence wasted Pt is deposited.^{24–27} Or the method require a complicated high temperature reduction step in a hydrogen atmosphere.²⁸ Recently, a most effective

^aDepartment of Materials Science and Engineering, Chair for Surface Science and Corrosion (WW4-LKO), Friedrich-Alexander-Universität Erlangen-Nürnberg, Martensstraße 7, 91058 Erlangen, Germany. E-mail: schmuki@ww4.uni-erlangen.de

^bResearch Laboratory Catalysis and Materials for the Environment and Processes (LRCMEP) Faculty of Sciences of Gabes (FSG), University of Gabes, University Campus, Erriadh City, 6072 Gabes, Tunisia

^cRegional Centre of Advanced Technologies and Materials, Palacky University, Šlechtitelů 27, 78371 Olomouc, Czech Republic

^dSchool of Chemical Engineering, Sichuan University, No. 24 South Section 1, Yihuan Road, Chengdu, 610065, China. E-mail: xuemeizhou@scu.edu.cn

^eLaboratoire des Substances Naturelles, Institut National de Recherche et d'Analyse Physico chimique, INRAP, Pôle Technologique de Sidi Thabet, 2020, Tunisia



reactive deposition approach was reported that delivers at very low amounts (<0.1 at%) highly active Pt SAs – these SAs were deposited by direct reaction of highly dilute chloroplatinic acid solutions ($\text{H}_2[\text{PtCl}_6]$) with $\text{g-C}_3\text{N}_4$.²⁹

Notably, the H_2 production rate of the low-loaded Pt SAs surpasses the activity of Pt SAs deposited using other techniques at a comparable or even higher loading.^{18,30,31} Or *vice versa*, some other studies achieve comparable activity levels, but they typically require more than ten times the Pt SA loading.^{18,29–32}

In reactive deposition approach, the reaction to anchored Pt SA consists of a sequence of (i) precursor hydrolysis, (ii) complex-adsorption, and finally (iii) a reaction with functional features on the surface of substrate. The adsorption of any Pt precursor is strongly affected by the speciation of the precursor in the solution. According to the “strong-electrostatic-adsorption” model,^{29,33,34} adsorption of a charged complex is mainly determined by the effective charge of the adsorbate species (the charge on the Pt-complex) and the charge of the surface (protonated or deprotonated surface hydroxyls). Both factors are primarily affected by the solution pH, but also by the ionic strength of the solution (shielding of surface charges), and by possible competitive adsorption. In practical terms, for adsorption of a Pt precursor, one either may select an anionic species (e.g., PtCl_6^{2-} at low pH (pH < PZC)), where the oxide surface is protonated and positively charged, or cationic species [e.g. $(\text{NH}_3)_4\text{Pt}^{2+}$, at high pH (pH > PZC)] where the surface is deprotonated and thus negatively charged.²⁴ Nevertheless, the situation is often much more complex, as the pH and background ions in solution also affect the hydrolysis of precursors and thus the speciation (and charge) of the adsorbing complex – for example Pt–Cl complexes can form positive, negative and neutral complexes in solution³⁵ that may be fully hydrolyzed by H_2O and OH^- . Moreover, the strength of adsorption forces can strongly be attenuated by the presence of background ions.

In a true direct reactive anchoring of Pt SAs, surface reaction step follows adsorption where ligand exchange but often also redox steps take place (as widely reported for $\text{H}_2[\text{PtCl}_6]$).^{24,27,36} The Pt SAs are primarily stabilized through coordination with N4 sites on $\text{g-C}_3\text{N}_4$, which ensures both high dispersion and stability of the Pt SAs under photocatalytic conditions.^{29,32,37–39}

Considering the broad range of factors that affect reactive adsorption, it is surprising that comparative investigations, namely on various Pt complex compounds, have hardly been carried out.^{40,41}

Therefore, in the present work we examine various Pt precursors to assess their suitability for creating active single atom species on $\text{g-C}_3\text{N}_4$. We select Pt precursors that differ in their chemical properties, such as oxidation state, Pt-coordination environment, and hydrolysis properties, and explore their feasibility to attach Pt SAs on $\text{g-C}_3\text{N}_4$. We then tried to understand the mechanism behind and evaluate loading and resulting reactivity in view of photocatalytic hydrogen production.

We first establish as a bench-mark, the conventionally used platinumic acid $\text{H}_2[\text{PtCl}_6]$ – then we explore $(\text{NH}_4)_2[\text{PtCl}_6]$,

$(\text{NH}_4)_2[\text{PtCl}_4]$, $\text{K}_2[\text{PtCl}_6]$, $\text{K}_2[\text{Pt}(\text{CN})_6]$, $\text{H}_2[\text{PtBr}_6]$, $\text{K}_2[\text{PtCl}_4]$, $\text{K}_2[\text{Pt}(\text{CN})_4]$, $[\text{Pt}(\text{NH}_3)_4]\text{Cl}_2$. We find that $\text{H}_2[\text{PtCl}_6]$, $(\text{NH}_4)_2[\text{PtCl}_6]$ and $(\text{NH}_4)_2[\text{PtCl}_4]$ are suitable for loading a significant amount of highly dispersed Pt SAs, all with a high hydrogen production efficiency. Optimized loading is observed from $(\text{NH}_4)_2[\text{PtCl}_6]$ solution (most effective at 2 mM) – without any solution adjustments. Best conditions for hydrogen evolution exhibit minimal ionic strength in solution, using Pt–chloro complexes (where the chloro-ligands react off during attachment). Redox processes during attachment of $\text{g-C}_3\text{N}_4$ are not key. Noteworthy is also that using cationic complex loading with $[\text{Pt}(\text{NH}_3)_4]\text{Cl}_2$ did not lead to satisfactory results for photocatalytic hydrogen evolution.

2. Results and discussion

We use for our investigations C_3N_4 synthesized by a well-established literature procedure from an equimolar mixture of melamine and dicyandiamide. Then the C_3N_4 powder is delaminated at 500 °C in air for 2 hours.^{42–44} After this treatment C_3N_4 presents a sheet-like structure with a layer thickness of ~18 nm, well in line with literature,^{8,29,45} and as evident from the scanning electron microscopy (SEM) image in Fig. 1a. These delaminated layers ($\text{g-C}_3\text{N}_4$) were then used as substrates and decorated with Pt-cocatalyst as SAs using an approach described in literature as “reactive deposition” (Pt SAs/ $\text{g-C}_3\text{N}_4$), and as described in more detail in the SI.^{26,27,46–48}

In a first set of experiments, we establish as a bench-mark, immersion of $\text{g-C}_3\text{N}_4$ in 2 mM $\text{H}_2[\text{PtCl}_6]$ for 1 h (details see also SI). Fig. 1b displays a high-resolution SEM image of the $\text{g-C}_3\text{N}_4$ after Pt deposition as SAs. The SEM image of Pt SAs/ $\text{g-C}_3\text{N}_4$ reveals no distinct particles, which is consistent with the deposition of non-aggregated single atoms, as the size is below the resolution limit of the SEM. Fig. 1c shows a high-angle annular dark-field scanning transmission electron microscopy (HAADF-STEM) image taken for Pt SAs/ $\text{g-C}_3\text{N}_4$, which reveals that the thin $\text{g-C}_3\text{N}_4$ layer is decorated with single atoms of Pt at a density of $8.8 \times 10^5 \mu\text{m}^{-2}$ (this value is determined by direct counting of individual Pt atoms within a defined area in a series of HAADF-TEM images, please see Fig. S1).

For reference, also samples with Pt nanoparticles (nominal loading of 3 wt%) on $\text{g-C}_3\text{N}_4$ were prepared (details in Experimental section). The SEM image in Fig. 1d shows nanoparticles that are clearly visible and the corresponding size distribution shows a relatively narrow range, with most particles centered around an average size of approximately 7 nm (see Fig. S2). This sample is annotated as Pt NPs/ $\text{g-C}_3\text{N}_4$ in the following sections.

X-ray photoelectron spectroscopy (XPS) of the Pt SA/ $\text{g-C}_3\text{N}_4$ sample shows in the Pt 4f region (Fig. 1e) a clear Pt doublet peak at a position of Pt 4f_{7/2} at 72.6 eV and Pt 4f_{5/2} at 76.0 eV, which is typical for Pt SA coordinated on the $\text{g-C}_3\text{N}_4$ surface^{29,49}—the peak position corresponds to a formal charge



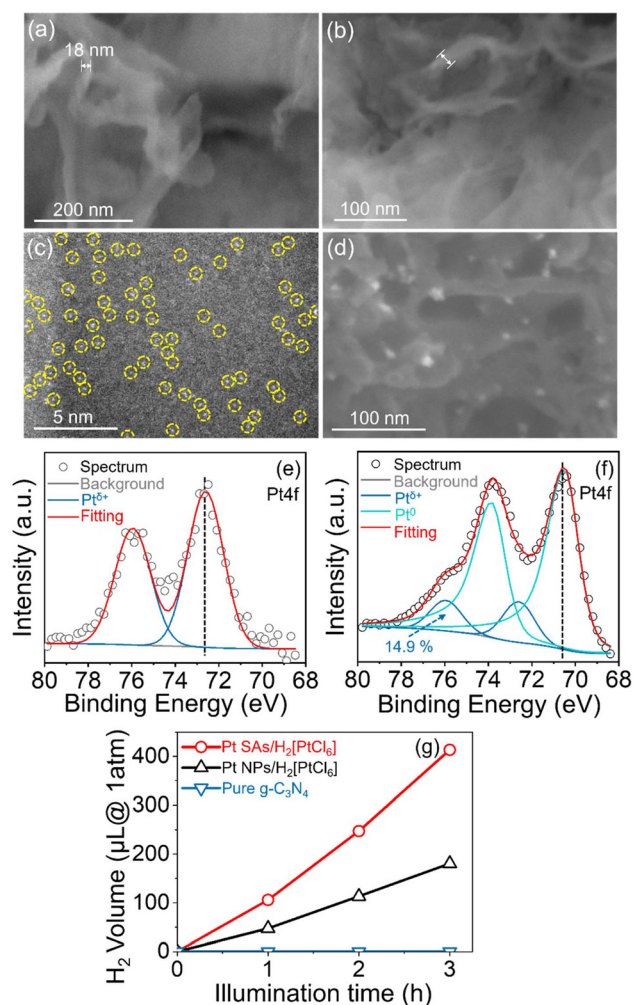


Fig. 1 (a) SEM image of pure $g\text{-C}_3\text{N}_4$; (b) SEM image of Pt SAs supported on $g\text{-C}_3\text{N}_4$; (c) HAADF-STEM image of Pt SAs/ $g\text{-C}_3\text{N}_4$; (d) SEM image of Pt NPs on $g\text{-C}_3\text{N}_4$; (e) XPS spectrum of Pt SAs/ $g\text{-C}_3\text{N}_4$; (f) XPS spectrum of Pt NPs/ $g\text{-C}_3\text{N}_4$; (g) photocatalytic H_2 evolution performance of Pt SAs/ $g\text{-C}_3\text{N}_4$, Pt NPs/ $g\text{-C}_3\text{N}_4$ (prepared using $\text{H}_2[\text{PtCl}_6]$ as the Pt precursor), and pure $g\text{-C}_3\text{N}_4$.

of Pt^{δ^+} with $\delta^+ \approx 2$. The observed oxidation state aligns with the anchoring of Pt SAs at nitrogen sites within $g\text{-C}_3\text{N}_4$, consistent with findings reported in previous studies.^{32,37–39} This

configuration is widely regarded as the catalytically active SA state responsible for facilitating the H_2 evolution reaction.^{50,51} In contrast, the XPS analysis of Pt NPs/ $g\text{-C}_3\text{N}_4$ (Fig. 1f) shows Pt $4f_{7/2}$ at 70.6 eV and Pt $4f_{5/2}$ at 73.9 eV, which corresponds to metallic Pt^0 (well in line with literature⁵²). From above considerations one can see that SEM (no detectable Pt nanoparticles) in combination with XPS (characteristic binding energy of Pt SAs) allows to indirectly confirm the presence of Pt single atoms on the $g\text{-C}_3\text{N}_4$ surfaces (this we used to screen deposits from different precursors as discussed further down). One may note that Cl ions are not detected from XPS Cl 2p spectra (Fig. S3c), which indicates that the Cl reacted off during dark deposition.

Then the photocatalytic H_2 generation activity of Pt SAs/ $g\text{-C}_3\text{N}_4$, Pt NPs/ $g\text{-C}_3\text{N}_4$, and neat $g\text{-C}_3\text{N}_4$ samples is evaluated in an electrolyte with a 10 vol% triethanolamine sacrificial agent in water (Fig. 1g), using a 365 nm LED light source (65 mW cm^{-2}). The H_2 evolution, for all samples, occurs linearly over the measured time, and the rates were thus determined from the slopes of the curves. Evidently, Pt SAs/ $g\text{-C}_3\text{N}_4$ exhibits a 2.3 times higher H_2 evolution rate compared to the Pt NPs/ $g\text{-C}_3\text{N}_4$ sample, which both provide a significantly higher activity than the neat $g\text{-C}_3\text{N}_4$. When the activity was normalized by Pt loading, the Pt SAs/ $g\text{-C}_3\text{N}_4$ showed an H_2 evolution rate of $1.7 \text{ mmol h}^{-1} (\text{mg Pt})^{-1}$, that is 10 times higher than the activity of Pt NPs/ $g\text{-C}_3\text{N}_4$ ($0.18 \text{ mmol h}^{-1} (\text{mg Pt})^{-1}$). Notably, in our previous study, XPS and SEM analyses confirmed that Pt remains atomically dispersed (δ^+ state) on $g\text{-C}_3\text{N}_4$ after photocatalytic H_2 evolution, with no observable metallic Pt NP formation.²⁹

Against this $\text{H}_2[\text{PtCl}_6]$ benchmark,²⁹ we tested a range of Pt-precursors as given in Table 1. Every Pt-salt was used at 2 mM aqueous solution, and immersion of $g\text{-C}_3\text{N}_4$ sample was done equal to the $\text{H}_2[\text{PtCl}_6]$ experiment. XPS and AAS were carried out to determine Pt loading and the results are given in Table 1, as well as the pH and the conductivity of the 2 mM salt solutions. For all samples after Pt loading and cleaning, the photocatalytic H_2 production activity was determined (Fig. 2). From XPS data in Table 1, Fig. S3 and S4 it is clear that only $\text{H}_2[\text{PtCl}_6]$, $(\text{NH}_4)_2[\text{PtCl}_6]$ and $(\text{NH}_4)_2[\text{PtCl}_4]$ lead to a considerable Pt loading while the other salts lead to no Pt loading or a Pt loading below the detection limit of XPS. In accord with these findings, for $\text{H}_2[\text{PtCl}_6]$ and $(\text{NH}_4)_2[\text{PtCl}_6]$ a

Table 1 Summary of the resulting Pt loadings, proportion of single-atom Pt, and photocatalytic H_2 evolution rate of Pt SAs/ $g\text{-C}_3\text{N}_4$ synthesized using different 2 mM Pt precursors, along with the pH and conductivity of the corresponding precursor solutions

Sample name	% SA	Pt loading (wt%) by AAS	Pt loading (at%) by XPS	pH	Conductivity ($\mu\text{S cm}^{-1}$)	H_2 evolution rate ($\mu\text{mol h}^{-1} \text{g}^{-1}$)
$\text{H}_2[\text{PtCl}_6]$	100	$0.0369 \pm 10\%$	0.07	2.3	1683	613
$(\text{NH}_4)_2[\text{PtCl}_6]$	100	$0.0262 \pm 10\%$	0.07	2.8	713	651
$(\text{NH}_4)_2[\text{PtCl}_4]$	100	$0.0188 \pm 10\%$	0.08	5.4	603	415
$\text{K}_2[\text{PtCl}_6]$	—	$0.0018 \pm 10\%$	<0.02	3.8	548	31
$\text{K}_2[\text{Pt}(\text{CN})_6]$	—	$0.0004 \pm 10\%$	<0.02	6.4	487	0
$\text{H}_2[\text{PtBr}_6]$	100	$0.0086 \pm 10\%$	<0.02	2.4	1353	120
$\text{K}_2[\text{PtCl}_4]$	100	$0.0048 \pm 10\%$	<0.02	5.5	584	136
$\text{K}_2[\text{Pt}(\text{CN})_4]$	—	$0.0006 \pm 10\%$	<0.02	6.8	437	13
$[\text{Pt}(\text{NH}_3)_4]\text{Cl}_2$	—	$0.0008 \pm 10\%$	<0.02	5.8	586	17



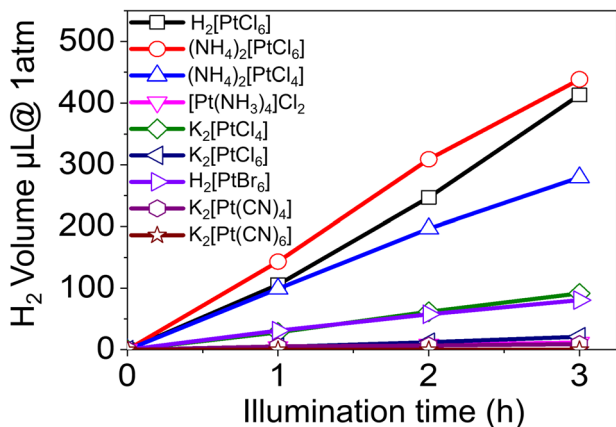


Fig. 2 Photocatalytic H₂ evolution performance of Pt SAs/g-C₃N₄ prepared with various Pt precursors.

considerably high H₂ evolution activity could be observed (Fig. 2). For all active samples, the XPS Pt peak shows the typical SA signature at 72.6 eV (Fig. S3a and b) (and no nanoparticles can be seen in SEM as shown in Fig. S5). XPS fitting and peak deconvolution shows an amount of $\approx 100\%$ SA contribution and no detectable contribution of Pt⁰.

Noteworthy is also that for all Pt⁴⁺ precursors the attached species is Pt^{δ+} with $\delta \approx 2$, *i.e.* a reduced species is formed and attached. In most of the cases, no ligand species (*e.g.*, Cl⁻) can be found, *i.e.*, in the attachment process these ligands are exchanged against nitrogen, either in the solution hydrolysis or in the surface attachment process.

From the comparison of the precursors, some important conclusions can be drawn. Namely, (i) that the exit group Cl⁻ or Br⁻ plays a very important role in the attachment of the Pt SA on the surface. H₂[PtCl₆] and H₂[PtBr₆] have a similar pH in the solution and provide a similar conductivity, *i.e.* the surface charge on the g-C₃N₄ and ionic strength of the solution are similar – nevertheless, the Br⁻ complex is hardly reacting with the surface (likely due to the more stable nature of the Pt–Br bond).⁵³ (ii) The redox process in the attachment reaction Pt⁴⁺ → Pt²⁺ is not a key factor in the attachment of SAs – this is evident from a similar loading and reactivity of using (NH₄)₂[PtCl₆] and (NH₄)₂[PtCl₄] onto g-C₃N₄, where Pt⁴⁺ and Pt²⁺ precursors are loaded as active (chloride-free) SAs. This suggests that for the Pt⁴⁺ precursor, reduction even may take place (*e.g.* by a red-ox process in the solution as has been suggested in literature³⁵) prior to the final surface attachment reaction.

The fact that many precursors do not show adsorption/reaction can be explained by comparing their solution pH (Table 1) with the PZC of g-C₃N₄. In literature^{54,55} and by the data in Fig. S6 one can determine a value of ≈ 3.5 – 4.5 for the g-C₃N₄ used in this study. This means that a significant adsorption (according to the SEA model) only occurs for anionic species at acidic pH below 4.0 (pH = 2.3 for H₂[PtCl₆], and pH = 2.8 for (NH₄)₂[PtCl₆]).

It is also interesting to note for (NH₄)₂[PtCl₄] that the pH of the solution is above 5.0 (pH = 5.4). The negatively charged surface indeed leads to adsorption/reaction with Pt²⁺, suggesting that the hydrolysis species of the precursor in the solution may matter, *i.e.*, the hydrolysis reaction may provide uncharged or even mildly positively charged species.^{35,56,57}

It is thus worthy to study the reverse adsorption, *i.e.* using a Pt-cation at elevated pH and compare the results to anionic loading. Thus, we tested [Pt(NH₃)₄]Cl₂ at various pH values where a positively charged [Pt(NH₃)₄]²⁺ is the adsorptive species present in the solution. Table 2 shows that for pH ≤ 9.0, no Pt species is detected by XPS and AAS, however with the increase of pH from 10.9 to 12.0, the loading of Pt increases, suggesting that the classic SEA is operative. Nevertheless, the amount of deposited Pt is low (at the detection limit of XPS) for every investigated pH. Also, the results from H₂ evolution (in 3 h) show that the hydrogen evolution activity is positively related to the loading of Pt (see Fig. 3 and Table 2) but due to the overall low loading of Pt, such photocatalyst is clearly less effective than the Pt deposited from anionic precursors under acidic conditions.

Moreover, if we inspect the data in Fig. 2 in detail, we find the highest activity (and the highest specific activity) for SAs deposited from (NH₄)₂[PtCl₆] (Fig. 4a). We evaluated the superior H₂ production efficiency over (NH₄)₂[PtCl₆] for a wide

Table 2 Summary of Pt loading of Pt SAs supported on g-C₃N₄, synthesized using 2 mM of [Pt(NH₃)₄]Cl₂ with pH adjustment, along with the conductivity of the corresponding precursor solutions

Sample name	% SA	Pt loading (at%) by XPS	Conductivity (µS cm ⁻¹)
[Pt(NH ₃) ₄]Cl ₂ , pH = 5.8	—	<0.02	586.2
[Pt(NH ₃) ₄]Cl ₂ , pH = 8.1	—	<0.02	582
[Pt(NH ₃) ₄]Cl ₂ , pH = 9	—	<0.02	579
[Pt(NH ₃) ₄]Cl ₂ , pH = 10.9	100	0.03	646
[Pt(NH ₃) ₄]Cl ₂ , pH = 12.0	100	0.06	1403

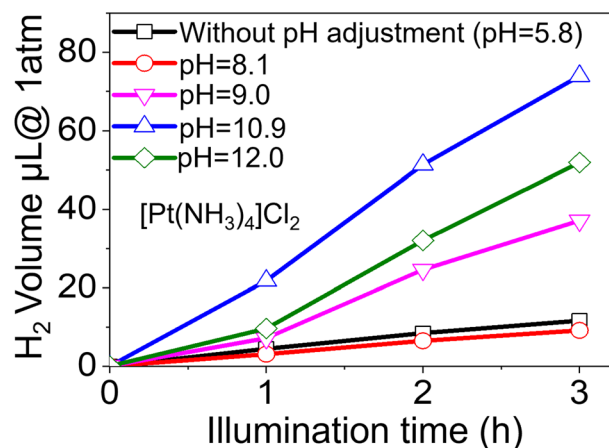


Fig. 3 Photocatalytic H₂ evolution performance of g-C₃N₄-supported Pt SAs synthesized from 2 mM [Pt(NH₃)₄]Cl₂ with pH adjustment.



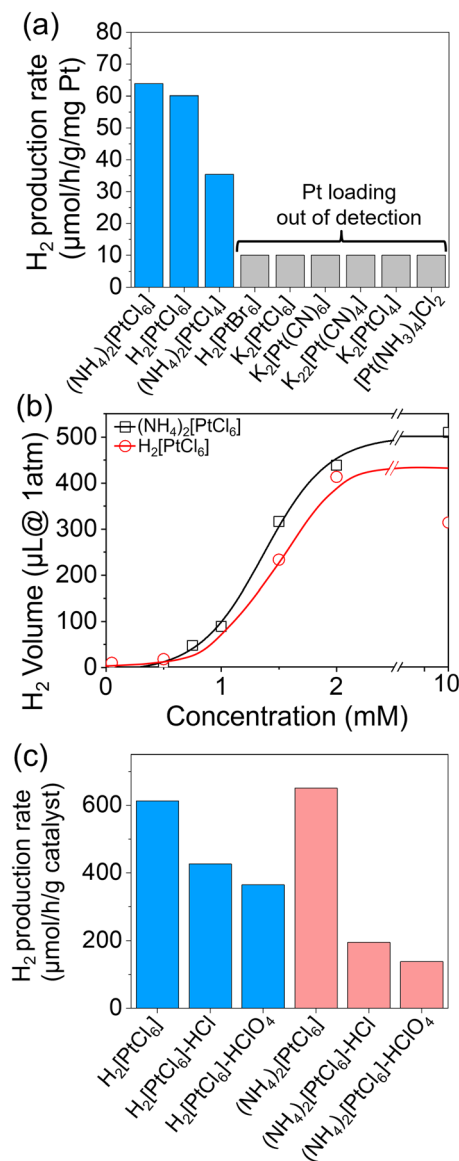


Fig. 4 (a) Normalized photocatalytic H₂ evolution performance of Pt SAs/g-C₃N₄ synthesized using different Pt precursors. (b) Photocatalytic activity as a function of precursor concentration for Pt SAs/g-C₃N₄ prepared using (NH₄)₂[PtCl₆] or H₂[PtCl₆]. (c) Bar diagram of H₂ evolution rates for Pt SAs/g-C₃N₄ synthesized with using (NH₄)₂[PtCl₆] or H₂[PtCl₆] at pH = 2, in comparison to Pt SAs/g-C₃N₄ synthesized with corresponding unmodified precursor solution.

concentration range (loading of samples given in Table S1), as illustrated in Fig. 4b. The highest hydrogen evolution rate is reached when the solution concentration is at 2 mM, further increase in the concentration of precursor (to 10 mM) does not lead to the increase of activity anymore.

Based on above considerations one may consider pH-adjustments to further improve the adsorption step. Therefore, we adjusted a 2 mM H₂[PtCl₆] solution and a (NH₄)₂[PtCl₆] solution to the same pH value of 2.0 using either HClO₄ (as “inert” acid) or HCl (affects the hydrolysis equilibrium also *via* Cl⁻). Evidently, both acids are detrimental for the loading of Pt and thus the hydrogen evolution activity (Table 3 and Fig. 4c), compared to the samples prepared without pH adjustment. The loading of Pt is half of the amount for H₂[PtCl₆] solution (0.0369 wt%) prepared using HCl (0.0148 wt%) or HClO₄ (0.0158 wt%) adjustment. Therefore, the adsorption behavior of anionic complexes, *e.g.* [PtCl₆]²⁻, under acidic conditions cannot be explained solely by the SEA mechanism. The impact of pH adjustment solution is even worse for (NH₄)₂[PtCl₆] precursors – the loading of Pt decreases to 0.0056 wt% using HCl and 0.0123 wt% using HClO₄, which may be ascribed to the fact that for (NH₄)₂[PtCl₆] more HCl or HClO₄ solution is needed to adjust pH, in order to buffer the NH₄⁺ ions in the solution. Or the protonation of surface groups by acid treatment may reduce the binding of platinum complexes.

Overall, the change in pH (by both acids) leads to significantly higher ionic strength (measured as conductivity), and this high ionic strength can provide a shielding effect for the negatively charged complex to deposit on the surface.⁵⁸ Or the pH in acidic solution leads to protonation of surface thus reduce the loading of Pt complex. Therefore, based on all above investigations, the photocatalysts prepared using (NH₄)₂[PtCl₆] precursor without pH adjustment gives the best hydrogen evolution activity, due to the most beneficial attachment of SAs on the C₃N₄. This is due to an ideal hydrolysis of this precursor in view of solution pH and ionic strength in the deposition solution, which is a result of both surface SEA and reactive deposition mechanism.

3. Conclusions

In the present work, we systematically explored the “reactive deposition” approach to anchor Pt SAs on g-C₃N₄ using various Pt precursors, revealing crucial insights into the critical factors affecting deposition and conditions required for

Table 3 Summary of Pt loading, proportion of single-atom Pt, and H₂ evolution rates for Pt SAs/g-C₃N₄ synthesized with 2 mM (NH₄)₂[PtCl₆] or H₂[PtCl₆] precursors at pH = 2, alongside the conductivity of the corresponding precursor solutions

Sample name	% SA	Pt loading (wt%) by AAS	Pt loading (at%) by XPS	pH	Conductivity (μS cm ⁻¹)	H ₂ evolution rate (μmol h ⁻¹ g ⁻¹)
H ₂ [PtCl ₆]-HCl	100	0.0148	0.05	2	3693	426
H ₂ [PtCl ₆]-HClO ₄	100	0.0158	0.04	2	3945	365
(NH ₄) ₂ [PtCl ₆]-HCl	—	0.0056	<0.02	2	4271	195
(NH ₄) ₂ [PtCl ₆]-HClO ₄	100	0.0123	0.11	2	63	138



optimal photocatalytic activity. Crucially, we demonstrate that both adsorption and subsequent surface reaction steps are essential to achieve effective reactive deposition. Our study highlights that anionic precursors significantly outperform cationic counterparts in adsorption on g-C₃N₄. Optimal conditions were identified at solution pH values below the point of zero charge (PZC \approx 3.5–4.5) of g-C₃N₄, combined with minimal ionic strength to prevent electrostatic shielding effects from background ions. Even relatively inert ions such as ClO₄[−] were found to notably impede active Pt precursor adsorption.

Furthermore, the choice of the leaving ligand in the Pt precursor dramatically influences deposition efficiency, with chloride complexes (Cl[−]) significantly surpassing bromide complexes (Br[−]), due to weaker Pt–Cl bond stability facilitating ligand exchange during attachment. Interestingly, redox processes associated with Pt⁴⁺ to Pt²⁺ reduction do not critically impact the deposition efficiency, as evidenced by comparable performance between Pt⁴⁺ and Pt²⁺ chloride precursors.

Among all tested precursors, (NH₄)₂[PtCl₆] emerged as the most effective, achieving superior catalytic activity with an optimized Pt loading of approximately 0.026 wt%. This precursor delivered an H₂ evolution rate surpassing even the widely employed H₂[PtCl₆] precursor under identical conditions. Additionally, adjusting precursor solutions to higher ionic strengths or significantly altering solution pH, negatively affected deposition efficiency and catalytic activity, underscoring the importance of maintaining suitable ionic strength conditions for optimal results.

Overall, this study provides critical insights into the parameters influencing Pt single atom deposition, offering a robust guideline for the development of highly efficient photocatalysts utilizing minimal Pt loading on g-C₃N₄.

Conflicts of interest

The authors declare no conflict of interest.

Data availability

The data supporting this article have been included as part of the supplementary information (SI). Supplementary information is available. See DOI: <https://doi.org/10.1039/d5nr03212a>.

Acknowledgements

The authors would like to acknowledge DFG and the Operational Program Research, Development and Education (European Regional Development Fund, Project No. CZ.02.1.01/0.0/0.0/15_003/0000416 of the Ministry of Education, Youth and Sports of the Czech Republic), the GA CR-EXPRO project (Grant No. 23-08019X) from the Czech Science Foundation for financial support. The authors would

also like to acknowledge the support of the Center for Nanoanalysis and Electron Microscopy (CENEM, Friedrich-Alexander-Universität Erlangen-Nürnberg).

References

- 1 K. Maeda, Photocatalytic Water Splitting Using Semiconductor Particles: History and Recent Developments, *J. Photochem. Photobiol., C*, 2011, **12**(4), 237–268, DOI: [10.1016/j.jphotochemrev.2011.07.001](https://doi.org/10.1016/j.jphotochemrev.2011.07.001).
- 2 K. Maeda and K. Domen, Photocatalytic Water Splitting: Recent Progress and Future Challenges, *J. Phys. Chem. Lett.*, 2010, **1**(18), 2655–2661, DOI: [10.1021/jz1007966](https://doi.org/10.1021/jz1007966).
- 3 K. Nakata and A. Fujishima, TiO₂ Photocatalysis: Design and Applications, *J. Photochem. Photobiol., C*, 2012, **13**(3), 169–189, DOI: [10.1016/j.jphotochemrev.2012.06.001](https://doi.org/10.1016/j.jphotochemrev.2012.06.001).
- 4 M. Sohail, S. Rauf, M. Irfan, A. Hayat, M. M. Alghamdi, A. A. El-Zahhar, D. Ghernaout, Y. Al-Hadeethi and W. Lv, Recent Developments, Advances and Strategies in Heterogeneous Photocatalysts for Water Splitting, *Nanoscale Adv.*, 2024, **6**(5), 1286–1330, DOI: [10.1039/D3NA00442B](https://doi.org/10.1039/D3NA00442B).
- 5 X. Li, J. Yu, J. Low, Y. Fang, J. Xiao and X. Chen, Engineering Heterogeneous Semiconductors for Solar Water Splitting, *J. Mater. Chem. A*, 2015, **3**(6), 2485–2534, DOI: [10.1039/c4ta04461d](https://doi.org/10.1039/c4ta04461d).
- 6 D. Bhandari, P. Lakhani and C. K. Modi, Graphitic Carbon Nitride (g-C₃N₄) as an Emerging Photocatalyst for Sustainable Environmental Applications: A Comprehensive Review, *RSC Sustainability*, 2024, **2**(2), 265–287, DOI: [10.1039/d3su00382e](https://doi.org/10.1039/d3su00382e).
- 7 G. Wu, Q. Wang, Q. Ren, Z. Mo and H. Xu, Molecular Structure Engineering of Graphitic Carbon Nitride for Photocatalytic Hydrogen Evolution: Recent Advances and Perspectives, *Small*, 2025, 2503954, DOI: [10.1002/sml.202503954](https://doi.org/10.1002/sml.202503954).
- 8 Y. Li, X. Li, H. Zhang, J. Fan and Q. Xiang, Design and Application of Active Sites in G-C₃N₄-Based Photocatalysts, *J. Mater. Sci. Technol.*, 2020, **56**, 69–88, DOI: [10.1016/j.jmst.2020.03.033](https://doi.org/10.1016/j.jmst.2020.03.033).
- 9 G. Dong, Y. Zhang, Q. Pan and J. Qiu, A Fantastic Graphitic Carbon Nitride (g-C₃N₄) Material: Electronic Structure, Photocatalytic and Photoelectronic Properties, *J. Photochem. Photobiol., C*, 2014, **20**, 33–50, DOI: [10.1016/j.jphotochemrev.2014.04.002](https://doi.org/10.1016/j.jphotochemrev.2014.04.002).
- 10 X. Yu, S. F. Ng, L. K. Putri, L. L. Tan, A. R. Mohamed and W. J. Ong, Point-Defect Engineering: Leveraging Imperfections in Graphitic Carbon Nitride (g-C₃N₄) Photocatalysts toward Artificial Photosynthesis, *Small*, 2021, **17**(48), 2006851, DOI: [10.1002/sml.202006851](https://doi.org/10.1002/sml.202006851).
- 11 C. Yang, Z. Xue, J. Qin, M. Sawangphruk, X. Zhang and R. Liu, Heterogeneous Structural Defects to Prompt Charge Shuttle in g-C₃N₄ Plane for Boosting Visible-Light Photocatalytic Activity, *Appl. Catal., B*, 2019, **259**, 118094, DOI: [10.1016/j.apcatb.2019.118094](https://doi.org/10.1016/j.apcatb.2019.118094).



- 12 M. Tahir, A. Sherryana, A. A. Khan, M. Madi, A. Y. Zerga and B. Tahir, Defect Engineering in Graphitic Carbon Nitride Nanotextures for Energy Efficient Solar Fuels Production: A Review, *Energy Fuels*, 2022, **36**(16), 8948–8977, DOI: [10.1021/acs.energyfuels.2c01256](https://doi.org/10.1021/acs.energyfuels.2c01256).
- 13 W. Che, W. Cheng, T. Yao, F. Tang, W. Liu, H. Su, Y. Huang, Q. Liu, J. Liu, F. Hu, Z. Pan, Z. Sun and S. Wei, Fast Photoelectron Transfer in (Cring)-C₃N₄ Plane Heterostructural Nanosheets for Overall Water Splitting, *J. Am. Chem. Soc.*, 2017, **139**(8), 3021–3026, DOI: [10.1021/jacs.6b11878](https://doi.org/10.1021/jacs.6b11878).
- 14 W.-J. Ong, L.-L. Tan, S.-P. Chai and S.-T. Yong, Heterojunction Engineering of Graphitic Carbon Nitride (g-C₃N₄) via Pt Loading with Improved Daylight-Induced Photocatalytic Reduction of Carbon Dioxide to Methane, *Dalton Trans.*, 2015, **44**(3), 1249–1257, DOI: [10.1039/C4DT02940B](https://doi.org/10.1039/C4DT02940B).
- 15 Y. Shiraishi, S. Kanazawa, Y. Sugano, D. Tsukamoto, H. Sakamoto, S. Ichikawa and T. Hirai, Highly Selective Production of Hydrogen Peroxide on Graphitic Carbon Nitride (g-C₃N₄) Photocatalyst Activated by Visible Light, *ACS Catal.*, 2014, **4**(3), 774–780, DOI: [10.1021/cs401208c](https://doi.org/10.1021/cs401208c).
- 16 S. A. Rawool, M. R. Pai, A. M. Banerjee, S. Nath, R. D. Bapat, R. K. Sharma, Jagannath, B. Dutta, P. A. Hassan and A. K. Tripathi, Superior Interfacial Contact Yields Efficient Electron Transfer Rate and Enhanced Solar Photocatalytic Hydrogen Generation in M/C₃N₄ Schottky Junctions, *ACS Appl. Mater. Interfaces*, 2023, **15**(33), 39926–39945, DOI: [10.1021/acsami.3c05833](https://doi.org/10.1021/acsami.3c05833).
- 17 C. Li, X. Dong, Y. Zhang, J. Hu, J. Yuan, G. Li, D. Chen and Y. Li, Micro-Tailored g-C₃N₄ Enables Ru Single-Atom Loading for Efficient Photocatalytic H₂ Evolution, *Appl. Surf. Sci.*, 2022, **596**, 153471, DOI: [10.1016/j.apsusc.2022.153471](https://doi.org/10.1016/j.apsusc.2022.153471).
- 18 Y. Hu, Y. Qu, Y. Zhou, Z. Wang, H. Wang, B. Yang, Z. Yu and Y. Wu, Single Pt Atom-Anchored C₃N₄: A Bridging Pt–N Bond Boosted Electron Transfer for Highly Efficient Photocatalytic H₂ Generation, *Chem. Eng. J.*, 2021, **412**, 128749, DOI: [10.1016/j.cej.2021.128749](https://doi.org/10.1016/j.cej.2021.128749).
- 19 J. Fonseca and J. Lu, Single-Atom Catalysts Designed and Prepared by the Atomic Layer Deposition Technique, *ACS Catal.*, 2021, **11**(12), 7018–7059, DOI: [10.1021/acscatal.1c01200](https://doi.org/10.1021/acscatal.1c01200).
- 20 A. Sanchez, S. Abbet, U. Heiz, W.-D. Schneider, H. Häkkinen, R. N. Barnett and U. Landman, When Gold Is Not Noble: Nanoscale Gold Catalysts, *J. Phys. Chem. A*, 1999, **103**(48), 9573–9578, DOI: [10.1021/jp9935992](https://doi.org/10.1021/jp9935992).
- 21 S. Eskandari, Y. Li, F. Tao and J. R. Regalbuto, The Use of Salts to Control Silica Supported Pt Particle Size in Charge Enhanced Dry Impregnation Syntheses, *Catal. Today*, 2019, **334**, 187–192, DOI: [10.1016/j.cattod.2018.11.033](https://doi.org/10.1016/j.cattod.2018.11.033).
- 22 F. J. Gracia, J. T. Miller, A. J. Kropf and E. E. Wolf, Kinetics, FTIR, and Controlled Atmosphere EXAFS Study of the Effect of Chlorine on Pt-Supported Catalysts during Oxidation Reactions, *J. Catal.*, 2002, **209**(2), 341–354, DOI: [10.1006/jcat.2002.3601](https://doi.org/10.1006/jcat.2002.3601).
- 23 R. W. Maatman and C. D. Prater, Adsorption and Exclusion in Impregnation of Porous Catalytic Supports, *Ind. Eng. Chem.*, 1957, **49**(2), 253–257, DOI: [10.1021/ie50566a040](https://doi.org/10.1021/ie50566a040).
- 24 S.-M. Wu and P. Schmuki, Single Atom Cocatalysts in Photocatalysis, *Adv. Mater.*, 2025, **37**(7), 2414889, DOI: [10.1002/adma.202414889](https://doi.org/10.1002/adma.202414889).
- 25 Y. Wang, N. Denisov, S. Qin, D. S. Gonçalves, H. Kim, B. B. Sarma and P. Schmuki, Stable and Highly Active Single Atom Configurations for Photocatalytic H₂ Generation, *Adv. Mater.*, 2024, **36**(25), 2400626, DOI: [10.1002/adma.202400626](https://doi.org/10.1002/adma.202400626).
- 26 S. Qin, J. Will, H. Kim, N. Denisov, S. Carl, E. Spiecker and P. Schmuki, Single Atoms in Photocatalysis: Low Loading Is Good Enough!, *ACS Energy Lett.*, 2023, **8**(2), 1209–1214, DOI: [10.1021/acsenerylett.2c02801](https://doi.org/10.1021/acsenerylett.2c02801).
- 27 Y. Wang, S. Qin, N. Denisov, H. Kim, Z. Bad'ura, B. B. Sarma and P. Schmuki, Reactive Deposition Versus Strong Electrostatic Adsorption (SEA): A Key to Highly Active Single Atom Co-Catalysts in Photocatalytic H₂ Generation, *Adv. Mater.*, 2023, **35**(32), 2211814, DOI: [10.1002/adma.202211814](https://doi.org/10.1002/adma.202211814).
- 28 D. Vasilchenko, A. Zhurenok, A. Saraev, E. Gerasimov, S. Cherepanova, L. Kovtunova, S. Tkachev and E. Kozlova, Platinum Deposition onto g-C₃N₄ with Using of Labile Nitratocomplex for Generation of the Highly Active Hydrogen Evolution Photocatalysts, *Int. J. Hydrogen Energy*, 2022, **47**(21), 11326–11340, DOI: [10.1016/j.ijhydene.2021.09.253](https://doi.org/10.1016/j.ijhydene.2021.09.253).
- 29 N. Lazaar, S. Wu, S. Qin, A. Hamrouni, B. B. Sarma, D. E. Doronkin, N. Denisov, H. Lachheb and P. Schmuki, Single-Atom Catalysts on C₃N₄: Minimizing Single Atom Pt Loading for Maximized Photocatalytic Hydrogen Production Efficiency, *Angew. Chem., Int. Ed.*, 2025, **64**(6), e202416453, DOI: [10.1002/anie.202416453](https://doi.org/10.1002/anie.202416453).
- 30 Y. Zuo, T. Li, N. Zhang, T. Jing, D. Rao, P. Schmuki, Š. Kment, R. Zbořil and Y. Chai, Spatially Confined Formation of Single Atoms in Highly Porous Carbon Nitride Nanoreactors, *ACS Nano*, 2021, **15**(4), 7790–7798, DOI: [10.1021/acsnano.1c01872](https://doi.org/10.1021/acsnano.1c01872).
- 31 L. Zhang, R. Long, Y. Zhang, D. Duan, Y. Xiong, Y. Zhang and Y. Bi, Direct Observation of Dynamic Bond Evolution in Single-Atom Pt/C₃N₄ Catalysts, *Angew. Chem., Int. Ed.*, 2020, **59**(15), 6224–6229, DOI: [10.1002/anie.201915774](https://doi.org/10.1002/anie.201915774).
- 32 X. Li, W. Bi, L. Zhang, S. Tao, W. Chu, Q. Zhang, Y. Luo, C. Wu and Y. Xie, Single-Atom Pt as Co-Catalyst for Enhanced Photocatalytic H₂ Evolution, *Adv. Mater.*, 2016, **28**(12), 2427–2431, DOI: [10.1002/adma.201505281](https://doi.org/10.1002/adma.201505281).
- 33 M. Schreier and J. R. Regalbuto, A Fundamental Study of Pt Tetraammine Impregnation of Silica: 1, The Electrostatic Nature of Platinum Adsorption, *J. Catal.*, 2004, **225**(1), 190–202, DOI: [10.1016/j.jcat.2004.03.034](https://doi.org/10.1016/j.jcat.2004.03.034).
- 34 J. E. Samad, S. Hoenig and J. R. Regalbuto, Synthesis of Platinum Catalysts over Thick Slurries of Oxide Supports by Strong Electrostatic Adsorption, *ChemCatChem*, 2015, **7**(21), 3460–3463, DOI: [10.1002/cctc.201500595](https://doi.org/10.1002/cctc.201500595).
- 35 W. A. Spieker, J. Liu, J. T. Miller, A. J. Kropf and J. R. Regalbuto, *An EXAFS Study of the Co-Ordination*



- Chemistry of Hydrogen Hexachloroplatinate(IV) 1. Speciation in Aqueous Solution*, 2002, vol. 232.
- 36 S. Hejazi, S. Mohajernia, B. Osuagwu, G. Zoppellaro, P. Andryskova, O. Tomanec, S. Kment, R. Zbořil and P. Schmuki, On the Controlled Loading of Single Platinum Atoms as a Co-Catalyst on TiO₂ Anatase for Optimized Photocatalytic H₂ Generation, *Adv. Mater.*, 2020, **32**(16), 1908505, DOI: [10.1002/adma.201908505](https://doi.org/10.1002/adma.201908505).
- 37 D. Deng, X. Chen, L. Yu, X. Wu, Q. Liu, Y. Liu, H. Yang, H. Tian, Y. Hu, P. Du, R. Si, J. Wang, X. Cui, H. Li, J. Xiao, T. Xu, J. Deng, F. Yang, P. N. Duchesne, P. Zhang, J. Zhou, L. Sun, J. Li, X. Pan and X. Bao, A Single Iron Site Confined in a Graphene Matrix for the Catalytic Oxidation of Benzene at Room Temperature, *Sci. Adv.*, 2025, **1**(11), e1500462, DOI: [10.1126/sciadv.1500462](https://doi.org/10.1126/sciadv.1500462).
- 38 A. Han, X. Wang, K. Tang, Z. Zhang, C. Ye, K. Kong, H. Hu, L. Zheng, P. Jiang, C. Zhao, Q. Zhang, D. Wang and Y. Li, An Adjacent Atomic Platinum Site Enables Single-Atom Iron with High Oxygen Reduction Reaction Performance, *Angew. Chem., Int. Ed.*, 2021, **60**(35), 19262–19271, DOI: [10.1002/anie.202105186](https://doi.org/10.1002/anie.202105186).
- 39 Y. Li, Z. Wang, T. Xia, H. Ju, K. Zhang, R. Long, Q. Xu, C. Wang, L. Song, J. Zhu, J. Jiang and Y. Xiong, Implementing Metal-to-Ligand Charge Transfer in Organic Semiconductor for Improved Visible-Near-Infrared Photocatalysis, *Adv. Mater.*, 2016, **28**(32), 6959–6965, DOI: [10.1002/adma.201601960](https://doi.org/10.1002/adma.201601960).
- 40 M. Wojnicki, K. Paclawski, R. P. Socha and K. Fitzner, Adsorption and Reduction of Platinum(IV) Chloride Complex Ions on Activated Carbon, *Trans. Nonferrous Met. Soc. China*, 2013, **23**(4), 1147–1156, DOI: [10.1016/S1003-6326\(13\)62577-7](https://doi.org/10.1016/S1003-6326(13)62577-7).
- 41 A. Topolski, Functionalization of Titania Nanotubes Surface with Platinum(II) Complexes, *Polyhedron*, 2023, **230**, 116218, DOI: [10.1016/j.poly.2022.116218](https://doi.org/10.1016/j.poly.2022.116218).
- 42 C. Marchal, T. Cottineau, M. G. Méndez-Medrano, C. Colbeau-Justin, V. Caps and V. Keller, Au/TiO₂-gC₃N₄ Nanocomposites for Enhanced Photocatalytic H₂ Production from Water under Visible Light Irradiation with Very Low Quantities of Sacrificial Agents, *Adv. Energy Mater.*, 2018, **8**(14), 1702142, DOI: [10.1002/aenm.201702142](https://doi.org/10.1002/aenm.201702142).
- 43 M. Karimi-Nazarabad, H. Ahmadzadeh and E. K. Goharshadi, Porous Perovskite-Lanthanum Cobaltite as an Efficient Cocatalyst in Photoelectrocatalytic Water Oxidation by Bismuth Doped g-C₃N₄, *Sol. Energy*, 2021, **227**, 426–437, DOI: [10.1016/j.solener.2021.09.028](https://doi.org/10.1016/j.solener.2021.09.028).
- 44 A. Torres-Pinto, M. J. Sampaio, C. G. Silva, J. L. Faria and A. M. T. Silva, Metal-Free Carbon Nitride Photocatalysis with in Situ Hydrogen Peroxide Generation for the Degradation of Aromatic Compounds, *Appl. Catal., B*, 2019, **252**, 128–137, DOI: [10.1016/j.apcatb.2019.03.040](https://doi.org/10.1016/j.apcatb.2019.03.040).
- 45 J. Fu, J. Yu, C. Jiang and B. Cheng, g-C₃N₄-Based Heterostructured Photocatalysts, *Adv. Energy Mater.*, 2018, **8**(3), 1701503, DOI: [10.1002/aenm.201701503](https://doi.org/10.1002/aenm.201701503).
- 46 S. Qin, N. Denisov, B. B. Sarma, I. Hwang, D. E. Doronkin, O. Tomanec, S. Kment and P. Schmuki, Pt Single Atoms on TiO₂ Polymorphs—Minimum Loading with a Maximized Photocatalytic Efficiency, *Adv. Mater. Interfaces*, 2022, **9**(22), 2200808, DOI: [10.1002/admi.202200808](https://doi.org/10.1002/admi.202200808).
- 47 S. Qin, N. Denisov, J. Will, J. Kolařík, E. Spiecker and P. Schmuki, A Few Pt Single Atoms Are Responsible for the Overall Co-Catalytic Activity in Pt/TiO₂ Photocatalytic H₂ Generation, *Sol. RRL*, 2022, **6**(6), 2101026, DOI: [10.1002/solr.202101026](https://doi.org/10.1002/solr.202101026).
- 48 Z. Wu, I. Hwang, G. Cha, S. Qin, O. Tomanec, Z. Badura, S. Kment, R. Zboril and P. Schmuki, Optimized Pt Single Atom Harvesting on TiO₂ Nanotubes—Towards a Most Efficient Photocatalyst, *Small*, 2022, **18**(2), 2104892, DOI: [10.1002/smll.202104892](https://doi.org/10.1002/smll.202104892).
- 49 Z. Zeng, Y. Su, X. Quan, W. Choi, G. Zhang, N. Liu, B. Kim, S. Chen, H. Yu and S. Zhang, Single-Atom Platinum Confined by the Interlayer Nanospace of Carbon Nitride for Efficient Photocatalytic Hydrogen Evolution, *Nano Energy*, 2020, **69**, 104409, DOI: [10.1016/j.nanoen.2019.104409](https://doi.org/10.1016/j.nanoen.2019.104409).
- 50 A.-P. Yan, Y.-J. Qiu, X.-E. Wang, G.-H. Wang, X.-K. Wei, X.-T. Li, X.-D. Chen, X. Shang, S.-L. Deng, J.-W. Zheng and S.-Y. Xie, Synergistic Promotion of Nitrogen Vacancies and Single Atomic Dopants on Pt/C₃N₄ for Photocatalytic Hydrogen Evolution, *iScience*, 2024, **27**(8), 110420, DOI: [10.1016/j.isci.2024.110420](https://doi.org/10.1016/j.isci.2024.110420).
- 51 C. Saetta, G. Di Liberto and G. Pacchioni, Water Splitting on a Pt₁/C₃N₄ Single Atom Catalyst: A Modeling Approach, *Top. Catal.*, 2023, **66**(15), 1120–1128.
- 52 D.-W. Sun, C.-C. Long and J.-H. Huang, Highly Dispersed Platinum-Anchored g-C₃N₄ Nanotubes for Photocatalytic Hydrogen Generation, *Int. J. Hydrogen Energy*, 2023, **48**(3), 943–952, DOI: [10.1016/j.ijhydene.2022.09.294](https://doi.org/10.1016/j.ijhydene.2022.09.294).
- 53 X. Cheng, Y.-L. Ye, L. Zhang, K.-W. Zheng, X.-H. Li and W.-M. Sun, A Theoretical Study of the Mono-Substituent Effect of Superhalogens on the Geometric Structure, Electronic Properties, and Hydrolysis of Cisplatin, *Chem. Phys.*, 2022, **555**, 111447, DOI: [10.1016/j.chemphys.2022.111447](https://doi.org/10.1016/j.chemphys.2022.111447).
- 54 B. Zhu, P. Xia, W. Ho and J. Yu, Isoelectric Point and Adsorption Activity of Porous g-C₃N₄, *Appl. Surf. Sci.*, 2015, **344**, 188–195, DOI: [10.1016/j.apsusc.2015.03.086](https://doi.org/10.1016/j.apsusc.2015.03.086).
- 55 T. L. Phung and T. K. G. Nguyen, Study on Synthesis of MoS₂ Modified g-C₃N₄ Materials for Treatment of Direct Black 38 Dye, *J. Viet. Env.*, 2018, **9**(3), 169–176.
- 56 E. H. Archibald and W. A. Gale, The Hydrolysis of Platinum Salts. Part II. Potassium Platinibromide, *J. Chem. Soc., Dalton Trans.*, 1922, **121**, 2849–2857.
- 57 E. H. Archibald, The Hydrolysis of Platinum Salts. Part I. Potassium Platinichloride, *J. Chem. Soc., Trans.*, 1920, **117**, 1104–1120.
- 58 M. Campinas and M. J. Rosa, The Ionic Strength Effect on Microcystin and Natural Organic Matter Surrogate Adsorption onto PAC, *J. Colloid Interface Sci.*, 2006, **299**(2), 520–529, DOI: [10.1016/j.jcis.2006.02.042](https://doi.org/10.1016/j.jcis.2006.02.042).

